Inorganic Chemistry

Article

pubs.acs.org/IC

Dual-Emissive Platinum(II) Metallacycles with Thiophene-Containing Bisacetylide Ligands

Yang Cao, Michael O. Wolf,* and Brian O. Patrick

Department of Chemistry, 2036 Main Mall, University of British Columbia, Vancouver, British Columbia V6T 1Z1, Canada

Ⓢ *Supporting Information*

ABSTRACT: Three *cis*-diphosphino Pt(II) metallacycles with thiophene-containing bisacetylide ligands were synthesized and their absorption and emission properties examined. These properties are explained by DFT and TD-DFT analysis of ground-state as well as singlet- and triplet-state energies and geometries. Two of the metallacycles show room-temperature dual emission (fluorescence and phosphorescence) with different intensity ratios. Replacing the phenylene or ethynylene groups with thiophene rings in the bisacetylide ligand of the metallacycles results in modulation of the S_1 and T_1 states to show stronger fluorescence and weaker phosphorescence. More rigid and planar metallacycles suffer less from energy loss due to smaller degrees of structural reorganization and thermal deactivation. These are important factors to consider when designing single-component dual-emissive materials for applications such as white-emitting OLEDs, self-referencing oxygen sensors, and hypoxia contrast agents.

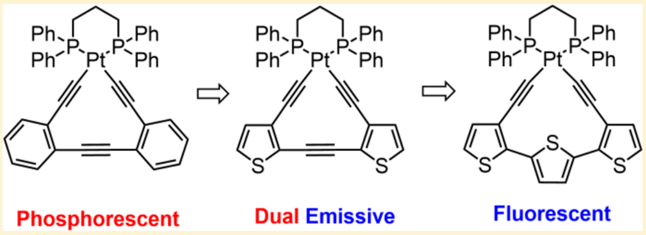

■ INTRODUCTION

Heavy atom-induced spin−orbit coupling (SOC) has been widely used to encourage intersystem crossing (ISC) in organic molecules from singlet excited states to triplet manifolds. For instance, iridium-containing dyes allow highly efficient ISC and emission from both the triplet and the singlet excited states, resulting in up to 100% internal efficiency in organic light-emitting devices (OLEDs) using these materials. This is significantly higher than the 25% efficiency limit of most fluorescent compounds that only emit from their singlet excited states.[1]

In molecules, SOC leads to the mixing of singlet and triplet wave functions with a coupling coefficient λ that is proportional to the spin−orbit coupling energy E_{SO} and inversely proportional to the corresponding singlet−triplet energy gap (E_S−E_T)

$$\lambda = E_{SO}/(E_S - E_T)$$

As a result of stronger SOC, the "spin flip" of the electron in molecules with heavier atoms becomes more favorable due to involvement of atomic orbitals with higher angular momentum. ISC is also much faster when corresponding frontier MOs of singlet and triplet states have a stronger contribution from heavy atoms.[2] Therefore, in molecules with heavy metal centers such as platinum(II), it is possible to attenuate ISC by varying the relative contribution of the metal atom in relevant MOs. Additionally, by tuning the singlet−triplet (E_S−E_T) energy gap, S_1 and T_1 states may both be populated upon excitation of the molecules. This also allows control over fluorescence/phosphorescence (FL/PH) ratios which is potentially useful for various important applications such as white-emitting OLEDs,[3] ratiometric oxygen sensors,[4] and hypoxia imaging in biological systems.[5] Limiting the nonradiative decay rates (k_{NR}) is also crucial for these applications since such decay often results in degraded performance and device overheating.

Oligomers and polymers containing trans-substituted Pt(II) bisacetylide centers have broad applications in nonlinear optical materials, OLEDs, polymer solar cells, and other molecular electronics applications.[6] They typically exhibit high triplet yields and long-lived ligand-localized triplet excited states.[2a,7] In molecules containing [*trans*-Pt$(PR_3)_2$(−C≡C−Ar−C≡C−)] units (Scheme 1, left), replacing the phenylene aryl groups in **A1** with thiophene rings results in lower T_1 states in molecule **A2** with a relatively unchanged energy gap between S_1 and T_1 states. Similar effects were observed in both monomeric and polymeric materials, except that the E_S−E_T gap is smaller in the latter.[2a]

Scheme 1

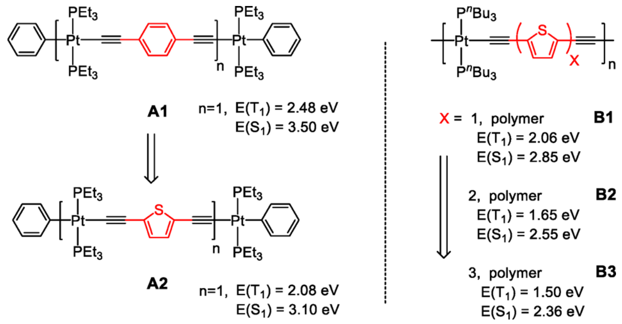

Received: June 17, 2016

DOI: 10.1021/acs.inorgchem.6b01464
Inorg. Chem. XXXX, XXX, XXX−XXX

In polymers **B1**, **B2**, and **B3**, relatively stronger fluorescence and weaker phosphorescence are observed when the ligand is extended in conjugation length from thiophene to bithiophene to terthiophene (Scheme 1, right). From **B1** to **B3**, the increasing number of thiophene rings reduces the influence of the heavy metal center that is mainly responsible for the intersystem crossing, making the T_1 state less accessible while the energy gap between S_1 and T_1 remains relatively constant.[8] Additionally, a longer conjugated system gives rise to a lower energy T_1 state, which makes ISC less efficient from higher singlet excited states (S_n). Therefore, S_1 states are relatively more efficiently populated than T_1 via fast internal conversion (IC) processes, resulting in stronger fluorescence.[8] These observations provide guidance to use similar strategies in platinum compounds to encourage stronger fluorescence, allowing room-temperature dual fluorescence (FL) and phosphorescence (PH) to be simultaneously observed with various FL/PH ratios.

Metallacycles containing *cis*-Pt bisacetylide metal centers were first reported almost two decades ago (Scheme 2);[9,10] they were found to give rise to very efficient ISC and thus have been considered good candidates as triplet sensitizers and for nonlinear optical applications.[11] Castellano et al. showed that such metallacycles show enhanced light absorption compared to their noncyclic analogues.[11b,c] Additionally, the more rigid cyclic structure gives rise to suppressed thermal deactivation and thus higher emission quantum efficiency. Therefore, *cis*-Pt bisacetylide metallacycles with higher stability and room-temperature tunable dual emission would be interesting for the applications discussed above and remain unknown to date.

Scheme 2. Metallacycles C1,[9] C2,[10] and C3[10] with Cis-Substituted Pt(II) Bisacetylide Metal Centers

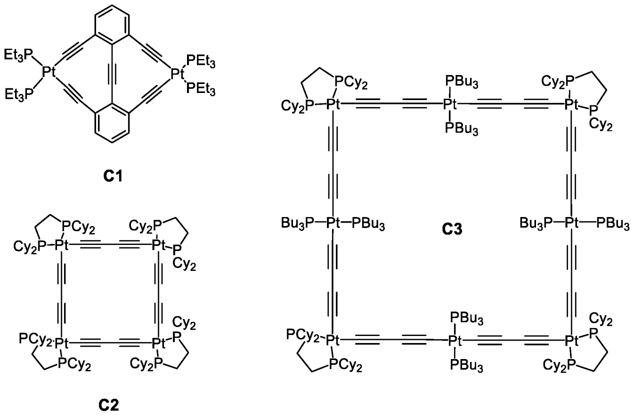

In this article, three new *cis*-Pt(II) bisacetylide metallacycles **1**, **2**, and **3** are discussed and compared with complex **4**[11c] previously reported by Castellano et al. (Scheme 3). Complex **4** provides an excellent starting point for these studies since it only shows green ligand-based phosphorescence at 497 nm in deaerated solutions. The effect of introducing thiophene rings at different positions in the ligand system while maintaining the cyclic structure is systematically explored by first replacing the two phenyl rings in **4** with thiophene rings to give complex **1**. Similarly, by introducing one additional thiophene ring to **1**, metallacycle **2** is formed. Finally, by changing the bridging acetylene in **4** to a thiophene ring, **3** is obtained. Complex **2** is found to fluoresce, while **1** and **3** show dual emission with varying FL/PH ratios.

Scheme 3

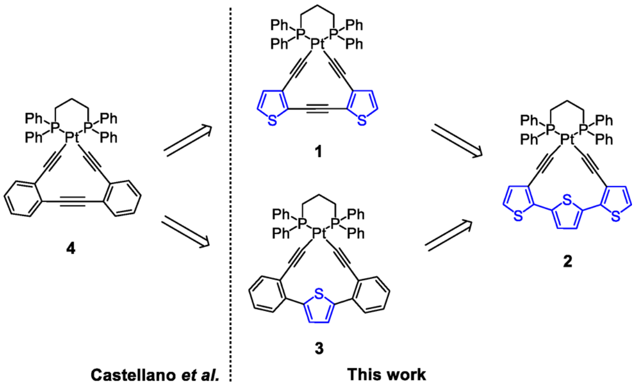

RESULTS AND DISCUSSION

Synthesis. Metallacycles **1**, **2**, and **3** were synthesized using a modification of Hagihara's method[12] using TMS-protected bidentate proligands **L1**, **L2**, and **L3**, respectively, as shown in Scheme 4. Alkynes were deprotected in situ and reacted with $Pt(dppp)Cl_2$ to incorporate the metal center with phosphine ancillary ligands. Pro-ligand **L2** was previously reported by our group,[13] and **L1** and **L3** were conveniently synthesized via Sonogashira reactions between trimethylsilylacetylene and the corresponding dibromo precursors in reasonable yields (Scheme 5).

Scheme 4. Synthesis of Metallacycles 1, 2, and 3

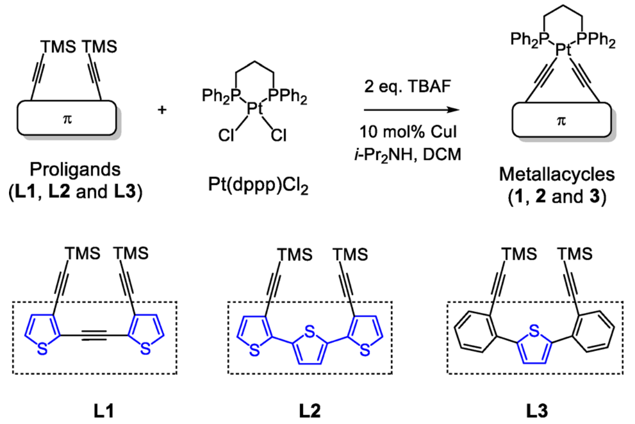

Solid-State Structures. Crystal structures of **1**, **2**, and **3** were obtained (Figures 1 and 2). As shown in Figure 2, complex **3** has two crystallographically distinct structures (A and B) in the unit cell each with different ligand conformations with multiple hydrogen bonds between them (Figure S1a). The metal centers in both structures A and B have almost identical C−Pt−C bond angles, unaffected by conformational differences in the relatively remote bisacetylide ligands. All metallacycles have square-planar geometries at the platinum centers, in line with other similar cis-substituted platinum bisacetylides in the literature.[9,10,14]

Compared with **2** and **3**, complex **1** has a smaller C−Pt−C bond angle of 84.8°, which indicates some degree of ring strain in this structure. While the bisacetylide ligands in **1** and **2** are only slightly twisted (S1−C4−C7−S2 torsion angle of 14.8° in **1**, dihedral angles between adjacent rings of 9.9° and 4.9° in **2**), the central thiophene ring in **3** is significantly out of the plane (dihedral angles between adjacent rings of 35.2° and 30.6° in

DOI: 10.1021/acs.inorgchem.6b01464

Scheme 5. Synthesis of Proligands

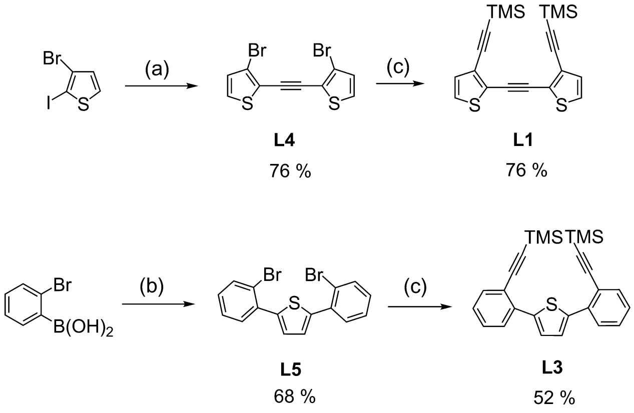

(a) CaC_2, H_2O, *cat.* $Pd(PPh_3)_4$, *cat.* CuI, CH_3CN/NEt_3, 50 °C.
(b) 2,5-diiodothiophene, K_2CO_3, *cat.* $Pd(PPh_3)_4$, THF/H_2O, 70 °C.
(c) Trimethylsilylacetylene, K_2CO_3, *cat.* $Pd(PPh_3)_4$, *cat.* CuI, $(i\text{-}Pr)_2NH$/toluene, reflux.

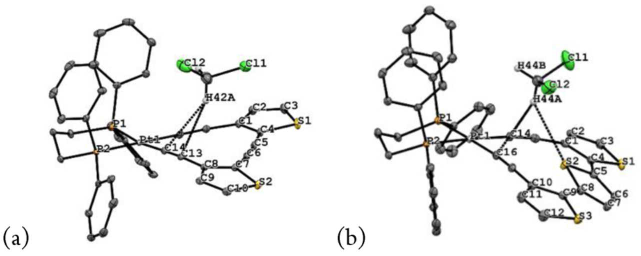

Figure 1. Perspective views of metallacycles (a) **1** and (b) **2** showing CH_2Cl_2 solvent molecules hydrogen bonding with each metallacycle. Thermal ellipsoids are shown at the 50% probability level; hydrogens on the metallacycles are omitted for clarity.

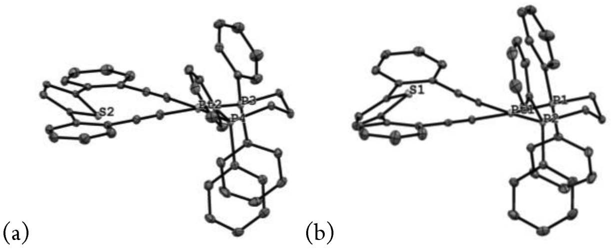

Figure 2. Perspective views of the two crystallographically distinct structures of complex **3**: (a) structure A and (b) structure B. Thermal ellipsoids are shown at the 50% probability level; hydrogens are omitted for clarity.

structure A; 26.0°and 25.5° in structure B). The crystals of **1**, **2**, and **3** all have CH_2Cl_2 solvent molecules in the crystal lattice. The CH_2Cl_2 molecules form hydrogen bonds with only one side of the ligand in **1**, while in **2** they bond to both sides of the ligand as well as with the sulfur atom on the central thiophene ring (with H44A). The CH_2Cl_2 molecules interact with **3** in a similar fashion to how they do with **2**; however, two protons are involved in this case (Figure S1b).

Electronic Absorption and Emission Spectra. The absorption spectra of **L1**, **L2**, and **L3** are shown in Figure 3a. The lowest energy absorption maxima of **L1** and **L3** are at 380 and 343 nm, respectively, in CH_2Cl_2. **L2** absorbs at higher wavelengths into the visible region, showing a maximum at 405 nm and a shoulder at ~430 nm. The resulting yellow color is attributed to the relatively smaller HOMO−LUMO gap of the $\pi-\pi^*$ transition on the more conjugated terthiophene moiety. The excitation spectra of **L1**, **L2**, and **L3** are shown in Figure 3b−d. All emission spectra show some vibrational fine structure. Emission maxima are at 392, 475, and 412 nm for **L1**, **L2**, and **L3**, respectively. **L1** has the smallest Stokes shift, indicating a smaller degree of geometrical relaxation in the excited state.

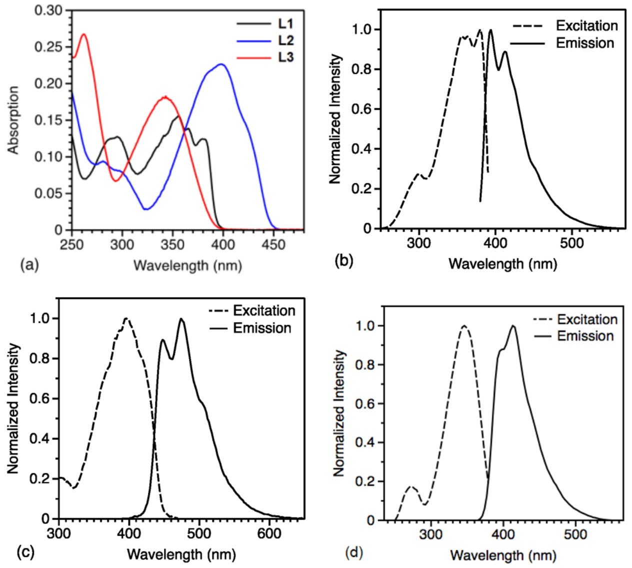

Figure 3. (a) UV−vis spectra of ligands **L1**, **L2**, and **L3** in CH_2Cl_2 (1.0×10^{-5} M), and excitation and emission spectra of **L1** (b), **L2** (c), and **L3** (d) in CH_2Cl_2 (1.0×10^{-5} M).

The absorption spectra of metallacycles **1**, **2**, and **3** in CH_2Cl_2 are shown in Figure 4. All complexes absorb strongly below 350 nm, attributed to high-energy localized $\pi-\pi^*$ transitions of the acetylene moieties. Complex **1** shows a lowest energy peak at 398 nm that is however red shifted

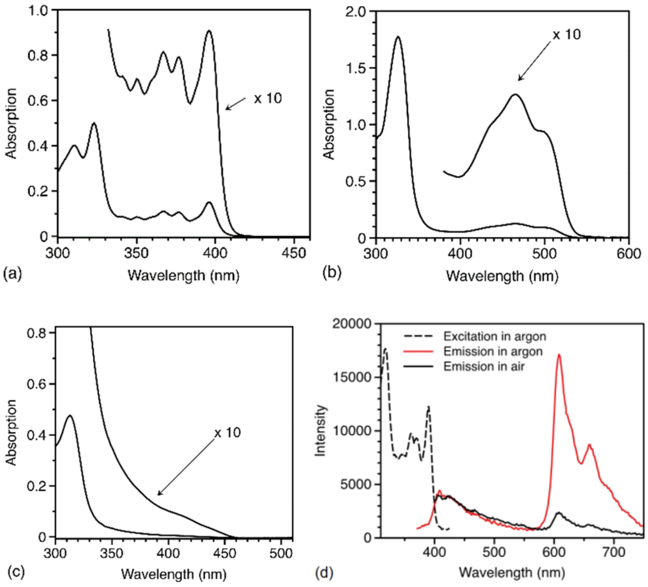

Figure 4. UV−vis spectra of metallacycles (a) **1**, (b) **2**, and (c) **3** in CH_2Cl_2 (1.0×10^{-5} M); (d) excitation spectrum of **1** with argon purging (emission @ 600 nm), and emission spectra under argon and air (excitation @ 390 nm).

approximately 20 nm relative to the absorption features of **L1**. The low-energy absorption shoulder of **2** is shifted to 500 nm, from 430 nm in **L2**, and **3** shows only a very weak feature tailing to 460 nm without a clear maximum, indicating the low oscillator strength between the S_0 and the S_1 states. In all cases, the metallacycle absorption is somewhat red shifted from the absorption of the proligands. This can be rationalized by restricted rotation and planarization of the structure upon formation of a bidentate chelate, resulting in more π conjugation which reduces the HOMO−LUMO gap.

The excitation and emission spectra of metallacycle **1** in CH_2Cl_2 are shown in Figure 4d. Compared with the purely phosphorescent analogue **4**,[11c] which emits at 497 nm, metallacycle **1** with two thiophene rings in the ligand instead of two *o*-phenylene groups shows significantly red-shifted phosphorescence at 610 nm and additionally a broad weak band between 400 and 550 nm. This relatively higher energy emission is considered to be fluorescence as assessed by its sensitivity to the presence of oxygen. This is suggestive of k_{ISC} to T_1 occurring on the same timescale as k_{FL}, slow enough so that both S_1 and T_1 states are effectively populated and emitting.

By contrast, metallacycle **2** containing three thiophene rings shows no phosphorescence (even at lower temperatures, Figure 5a), but instead bright yellow fluorescence is observed in solution (Figure 5b). Some terthiophene-containing structures are known to have low-lying nonemissive triplet states.[8,13] The nonradiative decay rate of triplet excited states increases exponentially as the triplet energy (T_1−S_0 gap) decreases, while nonradiative decay of S_1 is relatively energetically insensitive.[7a,15] Therefore, the absence of phosphorescence of **2** may be explained by the presence of a terthiophene-centered T_1 excited state that is very low in energy and only decays rapidly through nonradiative pathways.

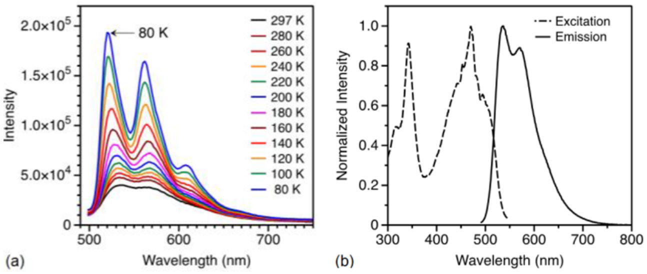

Figure 5. (a) Variable-temperature fluorescence spectra of **2** in a MeOH/EtOH medium, and (b) excitation and emission spectra of metallacycle **2** in air-equilibrated solution (1.0×10^{-5} M in CH_2Cl_2, excitation @ 460 nm and emission @ 540 nm).

In metallacycle **3** a single thiophene ring is introduced by replacing the central acetylene bridge in complex **4**, in anticipation of lowering the ligand-based triplet state and allowing both phosphorescence and fluorescence. Complex **3** can also be considered as an analog of **2** but with two phenyl rings replacing the outer thiophene rings. This change indeed gives rise to dual emission with a higher FL/PH ratio close to 1 (Figure 6). Interestingly, the phosphorescence of **3** is stronger with shorter excitation wavelengths compared to the fluorescence. After ruling out the possibility of contamination by trace amounts of residual emissive ligand, the possibility that higher singlet excited states (S_n) of **3** have stronger coupling with the T_1 state may be considered. When excited with higher energy light, these states are populated giving rise to faster ISC to T_1 and thus stronger phosphorescence. Similar effects are known in some platinum-containing conjugated polymers.[16]

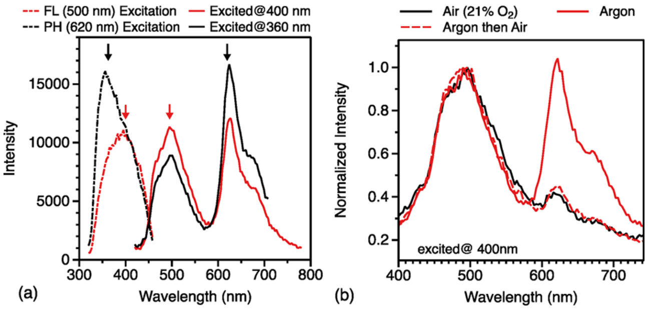

Figure 6. (a) Emission spectra of **3** under argon show two bands (500 and 620 nm), while excitation spectra of the two bands diverge at higher energy. (b) Emission of **3** in air, and dual emission under argon (excitation @ 400 nm).

Emission of both **1** and **3** is sensitive to oxygen, yet some phosphorescence remains in air-equilibrated solutions (Figures 4d and 6b). The phosphorescence is only completely quenched under pure O_2, which is beneficial for applications in high-concentration ratiometric O_2 sensing using unaffected fluorescence as a reference. Moreover, **1** and **3** have similar T_1−S_0 energy gaps as they phosphoresce at similar wavelengths. However, **3** fluoresces at a higher wavelength than **1** at 490 nm, indicating a lower-lying first singlet excited (S_1) state in **3**.

Electronic absorption and emission data including emission lifetimes (τ_{em}) and quantum yields (Φ_{em}) of the three metallacycles are collected in Table 1. All complexes show short fluorescence lifetimes of less than 1 ns, while **1** and **3** show relatively long phosphorescence with lifetimes of ~2 μs, indicating that k_{PH} is 3 orders of magnitude slower than k_{FL}. The fluorescence quantum efficiency of **2** is moderate, while **1** shows much weaker dual emission with a FL/PH ratio around 0.2. The FL/PH ratio of **3** is approximately 0.9 higher than that of **1**; however, the overall emission quantum efficiency is barely 1%.

Table 1. Electronic Absorption and Emission Data of Metallacycles in CH_2Cl_2 Solution

entry	λ_{abs} (nm)	λ_{FL} (nm)	Φ_{FL}	τ_{FL} (ns)	λ_{PH} (nm)	Φ_{PH}	τ_{PH} (μs)
1	398	405	0.011	0.70	610	0.053	2.23
2	500	536	0.15	0.45			
3	~400	490	0.0062	0.61	620	0.0054	1.97

By comparing **1** with **4** and **2** with **3** (Scheme 3), it is noted that replacing phenyl groups with thiophene rings in metallacycles can enhance fluorescence without adding extra conjugation. The difference between **1** and **2** demonstrates that adding conjugation length to the ligand leads to drastically increased fluorescence; however, the phosphorescence is diminished. It should be pointed out that although complexes **1** and **3** show many similarities, they are not directly comparable in an empirical way in the sense that only one type of group (C−C triple bond, benzene or thiophene ring) is replaced with another.

DFT and TD-DFT Simulations. DFT and TD-DFT calculations were carried out to help understand the photophysics of the metallacycles and simulate their ground- and excited-state properties. Optimized ground-state (S_0) geo-

DOI: 10.1021/acs.inorgchem.6b01464
Inorg. Chem. XXXX, XXX, XXX−XXX

metries of **1**, **2**, and **3** are shown in Table 2 (left column). Structure B was used for complex **3** due to its lower energy compared to structure A.

Table 2. DFT- and TD-DFT-Calculated Geometries of 1, 2, and 3 for S_0, S_1, and T_1 Electronic States

entry	S_0	S_1	T_1
1	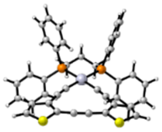	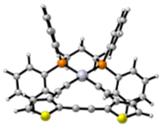	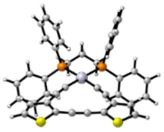
2	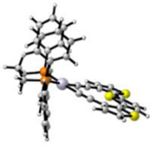		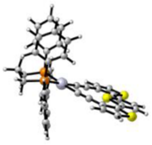
3	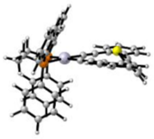	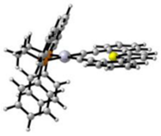	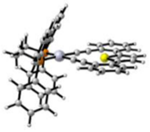

All structures show no symmetry (C_1) despite the presence of symmetric bisacetylide ligands. Complexes **1** and **2** show almost completely planar ligand geometries; however, the central thiophene ring in **3** still lies out of the plane by 44.5°. DFT-calculated geometry optimization of the lowest triplet state (T_1) of the metallacycles in CH_2Cl_2 solutions is shown in Table 2 (right column). TD-DFT-calculated optimized geometries of the first singlet excited state (S_1) of the metallacycles in CH_2Cl_2 solutions are presented in Table 2 (central column). All three metallacycles exhibit highly planar T_1 and S_1 excited-state structures.

Selected bond lengths in the optimized geometries of **1**, **2**, and **3** in different electronic states are shown in Table S1. In the ground state, all metallacycles show bond averaging between single and double bonds in the innermost ring. In **1** and **2**, the thiophene double bond is notably longer (1.40 Å) in the inner ring compared to the bonds in the outer ring (1.36 Å). These observations along with a downfield shift of the proton signal on the central thiophene ring of **2** (δ = 6.72 ppm compared with δ = 7.61 ppm in the proligand **L2**, both in $CDCl_3$), indicate the presence of "ring current" in the metallacycle.

At the S_1 and T_1 excited states, however, all metallacycles have almost perfectly planar ligand structures. This indicates that **3** undergoes significant planarization going from the GS to the S_1 or T_1 excited states, resulting in poor overlap between GS and excited-state MOs. It is also consistent with the very weak low-energy absorption features of this complex and may lead to the very low fluorescence and phosphorescence quantum efficiencies of **3** since nonradiative processes with low energy barriers become more favorable. Additionally, all metallacycles in the excited state show "quinoid-like" structure with reversed bond lengths for the single and double bonds relative to the GS geometry especially in T_1 (Table S1). It is also clear that the metallacycles **2** and **3** have much more in common between the excited states S_1 and T_1 than between GS and T_1/S_1 in terms of bond lengths and the geometry of the π-conjugated bisacetylide ligands.

The frontier orbitals of the ground-state metallacycles are presented in Table 3. All three complexes have π character localized on the ligand in the HOMO and π^* character in the LUMO. The HOMO and LUMO of **1** are uniformly distributed with some contributions from $5d_{xz}$ and $5d_{yz}$ orbitals on platinum yet are mostly comprised of π or π^* orbitals from the bisacetylide ligand. In metallacycles **2** and **3**, however, the LUMOs are strongly metal centered with contributions from empty $6p_z$ orbitals on platinum while the HOMOs are delocalized. This is indicative of the presence of ligand-to-metal charge transfer (LMCT) states in complexes **2** and **3**, which have previously been observed in conjugated Pt polymers with electron-rich ligands.[16,17]

The relative energies of metallacycles **1**, **2**, and **3** in T_1 and S_0 electronic states with T_1/S_0 geometries are summarized in Table S2. Metallacycle **2** has the lowest calculated T_1 state. The T_1-S_0 transition energies of 1.54 (0−0) and 1.17 eV (vertical) correspond to phosphorescence in the IR region (808 and 1060 nm), where fast thermal deactivation may render the T_1 state nonemissive at room temperature. Similarly, metallacycles **1** and **3** are calculated to exhibit phosphorescence with 0−0 transition energies of 1.89 and 2.06 eV, respectively, close to the experimental values at maximum intensity (2.02 and 1.99 eV). The relative energies of metallacycles **1**, **2**, and **3** in the S_1 and S_0 electronic states with S_1/S_0 geometries are summarized in Table S3. Vertical transition energies and oscillator strengths have also been calculated and are summarized in Table 4.

Table 3. Frontier Orbitals of Ground-State Metallacycles[a]

entry	1		2		3	
MOs	HOMO	LUMO	HOMO	LUMO	HOMO	LUMO
Top-down	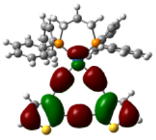	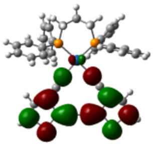	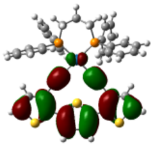	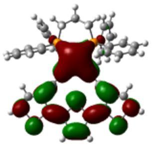	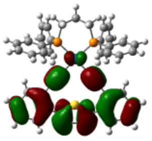	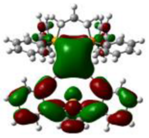
Side View	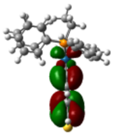	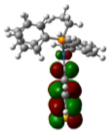	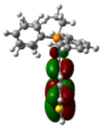		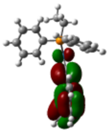	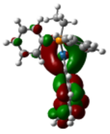

[a] Only the HOMO and LUMO are involved in the lowest energy $S_0 \rightarrow S_1$ electronic transitions for all three complexes.

DOI: 10.1021/acs.inorgchem.6b01464
Inorg. Chem. XXXX, XXX, XXX−XXX

Table 4. Vertical Excitation Energies of S_1 and T_1 States

entry	states	major transition	vertical transition energy (eV)	oscillator strength
1	S_1	HOMO−LUMO	3.10	0.169
	T_1	HOMO−LUMO	2.25	
2	S_1	HOMO−LUMO	2.44	0.100
	T_1	HOMO−LUMO	1.92	
3	S_1	HOMO−LUMO	3.22	0.001
	T_1	HOMO−LUMO	2.80	

These energies are used to construct energy diagrams of electronic states of metallacycles **1**, **2**, and **3** in Figure 7. From **1** to **3**, the decreasing oscillator strength of the vertical S_0−S_1 excitation is in line with the incrementally weaker molar extinction coefficients of the lowest energy absorption bands (Figure 4a−c). The T_1 state in **3** has a much higher vertical excitation energy but suffers more energy loss during relaxation to its lowest vibronic state: 0.74 eV is lost vs 0.36 eV in **1** and 0.38 eV in **2**. This may be related to the rotation of the thiophene ring between the ground state and the excited states.

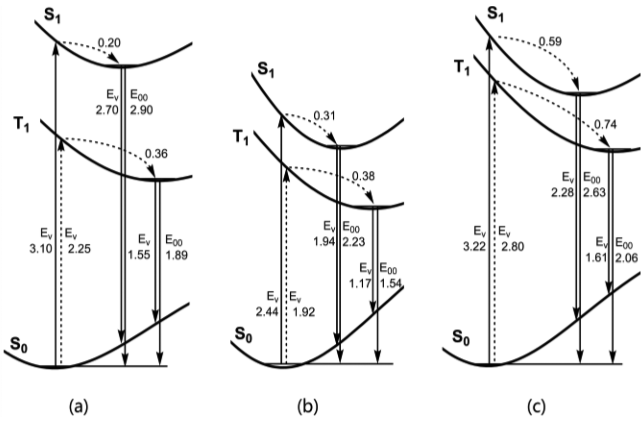

Figure 7. Summarized energy diagrams showing electronic transitions of metallacycles (a) **1**, (b) **2**, and (c) **3**. Energies shown in the above diagrams are in electron volts (eV) (E_v = vertical transition energy, E_{00} = 0−0 transition energy).

Calculated absorption and emission wavelengths are summarized in Table 5. Calculated absorption and triplet emission (phosphorescence) energies are in good agreement with the experimental values. Singlet emission energies were calculated using nonequilibrium solvation of the excited states, assuming vertical emission from relaxed S_1 states decaying with frozen geometry (i.e., vertical relaxation), yet large discrepancies with experimental data were observed. Interestingly the calculated emission assuming decay from a relaxed S_1 state to relaxed GS (i.e., 0−0 relaxation) agrees very well with the experimental values. Indeed, the vibronic fine structure in the fluorescence spectra of **2** at both room temperature and lower temperatures in Figure 5 shows that the first peak is always strongest in intensity. Therefore, the fluorescence maxima of **1**, **2**, and **3** are considered to be 0−0 emission instead of vertical transitions.

Table 5. Calculated Absorption and Emission Properties

	absorption wavelength (nm)		emission wavelength (nm)	
	$S_0 \rightarrow S_1$	$S_1 \rightarrow S_0$	$S_1 \rightarrow S_0$	$T_1 \rightarrow S_0$
entry	vertical	vertical	0−0	0−0
1	400 (398)[a]	459	428 (410)	655 (610)
2	508 (500)	639	557 (536)	
3	385 (~400)	544	471(485)	602 (620)
4[b]	329 (355)			497 (497)

[a] Experimental values given in parentheses. [b] Data for **4** from the literature.[11c]

■ EXPERIMENTAL SECTION

General. ^1H NMR, $^{13}C\{^1H\}$ NMR, and $^{31}P\{^1H\}$ NMR spectra were recorded on a Bruker Avance 400 (400 MHz) spectrometer. ^{31}P NMR chemical shifts are referenced to external 85% H_3PO_4, and other chemical shifts are referenced to the residual solvent signals. ESI mass spectra were measured in house using a Waters LC-MS ESI mass spectrometer. Infrared spectroscopy (IR) was performed on an attenuated total reflection (ATR) crystal using a PerkinElmer Frontier FTIR spectrometer. Absorption spectra were obtained on a Varian Cary 5000 UV-vis-NIR spectrophotometer, and emission measurements were performed on a PTI QuantaMaster 50 fluorimeter. Quantum yields were measured using a Labsphere general purpose integrating sphere. Phosphorescence lifetimes were recorded on a Horiba Jobin Yvon Fluorocube instrument equipped with a 370 nm nanosecond LED light source using time-correlated single-photon counting (TCSPC) collection. Fluorescence lifetimes were measured using a transient absorption and fluorescence lifetime measurement system with a Hamamatsu streak camera detector, a pulsed xenon cell light source, and a Pi-Acton spectrometer (200−900 nm spectral range) with a temporal range of 2 ns.

Synthesis. All syntheses were carried out under a dry N_2 atmosphere using standard Schlenk techniques. Dry toluene and tetrahydrofuran (THF) were purchased from Aldrich and purified by passing through towers containing activated alumina and molecular sieves under nitrogen. All other chemicals were purchased from commercial sources and used without further purification. Proligand **L2** (3,3″-bis(trimethylsilylethynyl)-2,2′:5′,2″-terthiophene, $TMS_2A_2T_3$)[13] and Pt(dppp)Cl_2[12] were synthesized using reported methods. **L1** and **L3** were conveniently synthesized from **L4** and **L5** via Sonogashira reactions. **L4**[18] and **L5**[19] were synthesized using methods different from those in the literature (Scheme 5).

***WARNING**: Flammable and explosive gas forms when calcium carbide becomes wet. Calcium carbide should be kept in a cool, dry, and well-ventilated place and away from heat and sources of ignition and handled carefully according to its Material Safety Data Sheet (MSDS).*

***L4** (Br_2TET), 1,2-Bis(3-bromothiophen-2-yl)ethyne.* CaC_2 (3.85 g, 60 mmol), $Pd(PPh_3)_4$ (1.16 g, 1.0 mmol), and CuI (380 mg, 2.0 mmol) were added to a round-bottom flask with a side arm under N_2. N_2-sparged CH_3CN (60 mL) was then added to the flask, followed by triethylamine (8.4 mL, 60 mmol) and 3-bromo-2-iodothiophene (3.70 g, 12.8 mmol). H_2O (1.1 mL, 60 mmol) was added slowly with stirring over 30 min, while the reaction temperature was maintained below 50 °C. The mixture was then kept at 50 °C using an oil bath and stirred overnight. Black insoluble solids were filtered off, and the solvent was removed from the filtrate under vacuum to obtain a brown-yellowish crude product. The pure product was obtained using flash column chromatography on silica (hexanes) as a white solid. Yield 1.70 g, 76%. The ^1H NMR and mass spectra matched with literature values.

***L5** (Br_2BTB), 2,5-Bis(2-bromophenyl)thiophene.* $Pd(PPh_3)_4$ (462 mg, 0.4 mmol), 2-bromophenylboronic acid (1.69 g, 8.4 mmol), 2,5-diiodothiophene (1.34 g, 4.0 mmol), and K_2CO_3 (2.32 g, 16.8 mmol) were added to a round-bottom flask with a stir bar under N_2. A N_2-sparged solvent mixture consisting of 20 mL of THF and 20 mL of deionized water was added to the flask with stirring. The mixture was slowly warmed to 70 °C and stirred for 18 h. The mixture was concentrated in vacuo to remove THF and extracted with diethyl ether (3 × 20 mL). The organic phases were combined, washed with water and brine, and dried over magnesium sulfate. The crude product was obtained after filtration and removal of the solvent under vacuum. The pure product was obtained using flash column chromatography on

DOI: 10.1021/acs.inorgchem.6b01464
Inorg. Chem. XXXX, XXX, XXX−XXX

silica (hexanes) as an off-white solid. Yield 1.08 g, 68%. ^1H NMR ($CDCl_3$, 400 MHz): δ 7.20 (td, J_1 = 10.4 Hz, J_2 = 2.2 Hz, 2H, 2 CH), 7.33−7.39 (m, 4H, 4 CH), 7.59 (dd, J_1 = 10.3 Hz, J_2 = 2.2 Hz, 2H, 2 CH), 7.72 (dd, J_1 = 10.6 Hz, J_2 = 1.3 Hz, 2H, CH). $^{13}C\{^1H\}$ NMR ($CDCl_3$, 100 MHz): δ 122.6 (C4, C−Br), 127.6 (CH, thienyl), 127.8 (CH, phenyl), 129.1 (CH, phenyl), 131.9 (CH, phenyl), 133.9 (CH, phenyl), 135.0 (CH, phenyl), 142.4 (CH, thienyl). Positive HRMS (APCI/ESI): m/z = 392.8944, $[M + H]^+$.

L1 (TMS$_2$A$_2$TET), 1,2-Bis(3-(trimethylsilylethynyl)thiophen-2-yl)ethyne. CuI (80 mg, 0.4 mmol), $Pd(PPh_3)_4$ (280 mg, 0.4 mmol), and **L4** (696 mg, 2.0 mmol) were added to a round-bottom flask with a stir bar under N_2. A N_2-sparged solvent mixture consisting of 15 mL of diisopropylamine and 30 mL of toluene was added to the flask with stirring, followed by trimethylsilylacetylene (471.5 mg, 4.8 mmol). The mixture was slowly warmed to 75 °C and stirred for 12 h. The reaction mixture was added to 30 mL of saturated NH_4Cl solution and extracted with ethyl acetate (4 × 20 mL). The organic phases were combined, washed with water and brine, and dried over magnesium sulfate. The brown crude product was obtained after filtration and removal of the solvent under vacuum. The pure product was obtained using flash column chromatography on silica (hexanes) as a light-yellow solid. Yield 580 mg, 76%. ^1H NMR ($CDCl_3$, 400 MHz): δ 0.28 (s, 18H, 6 CH_3), 7.03 (d, J = 5.3 Hz, 2H, CH), 7.19 (d, J = 5.2 Hz, 2H, CH). $^{13}C\{^1H\}$ NMR ($CDCl_3$, 100 MHz): δ 0.1 (CH_3), 89.8 (C4, $C\equiv C$), 98.8(C4, $C\equiv C$), 99.7 (C4, $C\equiv C$), 126.7 (CH, thienyl), 127.0 (C4, thienyl), 127.1 (C4, thienyl), 129.8 (CH, thienyl). Positive HRMS (APCI/ESI): m/z = 383.0774, $[M + H]^+$. FTIR (ATR) = 2152 cm^{-1} ($\nu_{C\equiv C}$).

L3 (TMS$_2$A$_2$BTB), 2,5-Bis(2-(trimethylsilylethynyl)phenyl)thiophene. The same reaction conditions, workup procedure, and purification method were used for **L1** except that **L5** was used as the starting material instead of **L4**. A pale-yellow solid was obtained after column purification in 52% yield. ^1H NMR ($CDCl_3$, 400 MHz): δ 0.29 (s, 18H, 6 CH_3), 7.23 (td, J_1 = 7.6 Hz, J_2 = 1.2 Hz, 2H, CH), 7.35 (td, J_1 = 7.6 Hz, J_2 = 1.4 Hz, 2H, CH), 7.59−7.64 (m, 4H, 2 CH), 7.79 (s, 2H, CH). $^{13}C\{^1H\}$ NMR ($CDCl_3$, 100 MHz): δ −0.1 (CH_3), 99.7 (C4, $C\equiv C$), 105.2 (C4, $C\equiv C$), 120.2 (C4, phenyl), 127.0 (CH, phenyl), 127.4 (CH, phenyl), 128.6 (CH, phenyl), 129.0 (CH, phenyl), 134.6 (CH, thienyl), 135.9 (C4, phenyl), 142.2 (C4, thienyl). Positive HRMS (APCI/ESI): m/z = 429.1522, $[M + H]^+$. FTIR (ATR) = 2150 cm^{-1} ($\nu_{C\equiv C}$).

Complex 1, Pt(dppp)A$_2$TET. Proligand **L1** (193 mg, 0.505 mmol), $Pt(dppp)Cl_2$ (339 mg, 0.500 mmol), and CuI (10 mg, 0.05 mmol) were added to a round-bottom flask with a stir bar under N_2. Then 30 mL of a N_2-sparged solvent mixture consisting of 15 mL of diisopropylamine and 15 mL of CH_2Cl_2 was added to the flask with stirring. A solution of 1.0 M tetrabutylammonium fluoride (TBAF, 2.1 mL, 2.1 mmol) in THF was slowly added to the mixture over 30 min, and the resulting solution was stirred for 18 h. Solvents were removed under vacuum to give the crude mixture, which was then purified using flash column chromatography on silica (20% $CHCl_3$ in hexanes, v/v) to give the pure product as a yellow powder. Yield 282 mg, 67%. ^1H NMR (CD_2Cl_2, 400 MHz): δ 2.00−2.11 (m, 2H, CH_2), 2.62 (br, 4H, $2CH_2$), 6.51 (d, J = 5.2 Hz, 2H, 2 CH), 7.10 (d, J = 5.2 Hz, 2H, 2 CH), 7.39−7.44 (m, 12H, 12 CH), 7.77−7.82 (m, 8H, 8 CH). $^{31}P\{^1H\}$ NMR (CD_2Cl_2, 162 MHz): δ −6.92 (J_{Pt-P} = 2215 Hz). Positive ESI-TOF: m/z = 843.0982, $[C_{41}H_{31}S_2P_2{}^{194}Pt + H]^+$. FTIR (ATR) = 2095 cm^{-1} ($\nu_{C\equiv C}$).

Complex 2, Pt(dppp)A$_2$T$_3$. The same procedure used for **1** was employed except proligand **L2** was used instead. An orange powder was obtained as the pure product. Yield 288 mg, 64%. ^1H NMR (CD_2Cl_2, 400 MHz): δ 1.93−2.06 (m, 2H, CH_2), 2.56−2.60 (m, 4H, $2CH_2$), 5.95 (d, J = 5.2 Hz, 2H, 2 CH), 6.72 (s, 2H, 2 CH), 6.74 (d, J = 5.2 Hz, 2H, 2 CH), 7.41−7.44 (m, 12H, 12 CH), 7.67−7.72 (m, 8H, 8 CH). $^{31}P\{^1H\}$ NMR (CD_2Cl_2, 162 MHz): δ −5.99 (J_{Pt-P} = 2177 Hz). Positive ESI-TOF: m/z = 923.0652, $[C_{43}H_{32}S_3P_2{}^{194}Pt + Na]^+$. FTIR (ATR) = 2098 cm^{-1} ($\nu_{C\equiv C}$).

Complex 3, Pt(dppp)A$_2$BTB. The same procedure used for **1** was employed except proligand **L3** was used instead. A yellow powder was obtained as the pure product. Yield 249 mg, 56%. ^1H NMR ($CDCl_3$, 400 MHz): δ 2.02−2.17 (m, 2H, CH_2), 2.52 (br, 4H, $2CH_2$), 6.23 (dd, J_1= 7.7 Hz, J_2= 0.9 Hz, 2H, 2 CH), 6.78 (td, J_1= 7.6 Hz, J_2= 1.2 Hz, 2H, 2 CH), 6.98 (s, 2H, 2CH), 7.00 (td, J_1= 7.6 Hz, J_2= 1.2 Hz, 2H, 2 CH), 7.35−7.42 (m, 14H, 14 CH), 7.70−7.72 (m, 8H, 8 CH). $^{31}P\{^1H\}$ NMR ($CDCl_3$, 162 MHz): δ −5.58 (J_{Pt-P} = 2183 Hz). Positive ESI-TOF: m/z = 889.1721, $[C_{47}H_{37}SP_2{}^{194}Pt + H]^+$. FTIR (ATR) = 2105 cm^{-1} ($\nu_{C\equiv C}$).

X-ray Crystallography. Crystals of **1**, **2**, and **3** suitable for single-crystal X-ray diffraction were obtained by diffusion of pentane into solutions of the complexes in CH_2Cl_2 or CH_2Cl_2/CH_3CN mixed solvent. X-ray diffraction data were collected with a Bruker X8 APEX II diffractometer with graphite-monochromated Mo Kα radiation. Data were collected and integrated using the Bruker SAINT[20] software package. Data were corrected for absorption effects using the multiscan technique (SADABS).[21] The data were corrected for Lorentz and polarization effects. The structures were solved by direct methods.[22] All non-hydrogen atoms were refined anisotropically. All hydrogen atoms were placed in calculated positions. Selected bond lengths and bond angles are summarized for **1** and **2** (Table S4) and two crystallographically independent structures of **3** (Table S5).

1·CH_2Cl_2 crystallizes with one disordered CH_2Cl_2 solvent molecule in the asymmetric unit. The structure is in the $P2_1/n$ space group, with a primitive monoclinic unit cell containing four molecules of **1**. **2**·1.2[CH_2Cl_2]·0.8CH_3CN crystallizes with one complete CH_2Cl_2 molecule as well as one site that is partially occupied by CH_2Cl_2 and also by CH_3CN (~1:4) in the asymmetric unit. The structure is in the P-1 space group, with a primitive triclinic unit cell containing two **2** molecules. **3**·CH_2Cl_2 crystallizes with two crystallographically independent molecules in the asymmetric unit. Additionally, there are two molecules of CH_2Cl_2 in the asymmetric unit. The structure is in the $P2_1/n$ space group with a primitive monoclinic unit cell containing eight molecules of **3**.

DFT Stimulations. Density functional theory (DFT) calculations were carried out using the Gaussian 09 Rev.D01 suite of programs.[23] The PBE0 hybrid functional[24] with 6-31G* basis set (for C, H, S, and P atoms) and the LANL2DZ effective-core pseudopotential[25] (for Pt) was employed to simulate the ground-state (S_0) and T_1 structure of all three metallacycles. Triplet states are treated using unrestricted formalism. Structural coordinates from X-ray crystallography were used as starting points of geometry optimizations. Optimized structures were confirmed to be the minimum on the potential energy surface by vibrational frequency calculations. Time-dependent DFT (TD-DFT) calculations were also performed to understand S_1 excited-state electronics and the absorption and emission behaviors of these complexes. For all simulations, a solvation effect of CH_2Cl_2 (ε = 8.93) was implemented using the polarizable continuum model[26] (PCM) in Gaussian 09.

Frequency calculations on **1**, **2**, and **3** in their optimized geometries confirmed that they are on the global minimum on the potential energy surface. Frequency calculations also give some insight into their IR absorptions. They are predicted to show symmetric and antisymmetric stretching modes where vibrations of the two $C\equiv C$ bonds are in phase or out of phase, respectively. The antisymmetric mode is calculated to have a much weaker IR absorption than the symmetric mode. Experimentally, only one peak is observed in **1**, **2**, and **3**. The same goes for compound **4** in the literature.[11c] This may be due to the constrained geometry in cyclic structures as similar acyclic *cis*-Pt(II) bisacetylides show two peaks.[27] After applying an empirical scaling factor of 0.95 (for the PBE0 hybrid functional and 6-31G* basis set),[28] the predicted IR frequencies are reasonably close to experimental values (Table S6). Small discrepancies may be attributed to the PCM solvation assumptions used in DFT calculations, while IR spectra were recorded in the solid state using powder samples.

CONCLUSIONS

In summary, we prepared and characterized three different thiophene-containing Pt metallacycles **1**, **2**, and **3** with dppp ancillary ligands. Crystal structures show that they all possess square-planar metal centers with similar metallacycle ring size.

In solution, both phosphorescence and fluorescence are attributed to ligand-based excited states. It is confirmed that replacing phenyl groups with thiophene rings in metallacycles can induce or enhance fluorescence without adding extra conjugation to the ligand, thus obtaining room-temperature dual emission with different FL/PH ratios. It is also revealed that adding thiophene rings to extend the conjugation length in metallacycles (from **1** to **2**) will likely shut down phosphorescence due to ligand-based low-lying nonemissive T_1 states.

DFT and TD-DFT calculations show that upon excitation from S_0 to S_1, **2** and **3** undergo charge transfer from the ligand to the empty 6p_z orbital of the Pt atom while **1** shows only $\pi-\pi^*$ transitions. It is also revealed that all three metallacycles show very planar quinoid-like structure in the S_1 and T_1 excited state with contracted single bonds and lengthened double/triple bonds in the ligand. Complex **3** undergoes significant planarization going from the GS to the S_1 or T_1 excited states, resulting in weaker absorbance and much larger energy loss in vibrational relaxation processes compared to **1** and **2**. Both fluorescence and phosphorescence maxima of these metallacycles are attributed to 0−0 relaxation from corresponding relaxed S_1 and T_1 excited states and match up with calculated values. We anticipate the above findings may be useful for future applications of these types of complexes in single-component white-emitting OLEDs, self-referencing oxygen sensors, and hypoxia contrast agents.

■ ASSOCIATED CONTENT

Ⓢ Supporting Information

The Supporting Information is available free of charge on the ACS Publications website at DOI: 10.1021/acs.inorgchem.6b01464.

Supplementary crystallographic and DFT/TD-DFT data (PDF)

X-ray crystallographic data for metallacycle **1** (CIF)

X-ray crystallographic data for metallacycle **2** (CIF)

X-ray crystallographic data for metallacycle **3** (CIF)

■ AUTHOR INFORMATION

Corresponding Author

*E-mail: mwolf@chem.ubc.ca.

Notes

The authors declare no competing financial interest.

■ ACKNOWLEDGMENTS

We thank the Natural Sciences and Engineering Research Council of Canada for funding this research.

■ REFERENCES

(1) (a) Adachi, C.; Baldo, M. A.; Thompson, M. E.; Forrest, S. R. *J. Appl. Phys.* **2001**, *90*, 5048. (b) Lamansky, S.; Djurovich, P.; Murphy, D.; Abdel-Razzaq, F.; Lee, H. E.; Adachi, C.; Burrows, P. E.; Forrest, S. R.; Thompson, M. E. *J. Am. Chem. Soc.* **2001**, *123*, 4304. (c) Sun, Y.; Giebink, N. C.; Kanno, H.; Ma, B.; Thompson, M. E.; Forrest, S. R. *Nature* **2006**, *440*, 908.

(2) (a) Köhler, A.; Beljonne, D. *Adv. Funct. Mater.* **2004**, *14*, 11. (b) Samonina-Kosicka, J.; DeRosa, C. A.; Morris, W. A.; Fan, Z.; Fraser, C. L. *Macromolecules* **2014**, *47*, 3736. (c) Kozhevnikov, D. N.; Kozhevnikov, V. N.; Shafikov, M. Z.; Prokhorov, A. M.; Bruce, D. W.; Gareth Williams, J. A. *Inorg. Chem.* **2011**, *50*, 3804.

(3) (a) Glazer, E. C.; Magde, D.; Tor, Y. *J. Am. Chem. Soc.* **2005**, *127*, 4190. (b) Zhou, C.; Tian, Y.; Yuan, Z.; Han, M.; Wang, J.; Zhu, L.; Tameh, M. S.; Huang, C.; Ma, B. *Angew. Chem., Int. Ed.* **2015**, *54*, 9591. (c) Han, M.; Tian, Y.; Yuan, Z.; Zhu, L.; Ma, B. *Angew. Chem., Int. Ed.* **2014**, *53*, 10908.

(4) (a) Xiang, H.; Zhou, L.; Feng, Y.; Cheng, J.; Wu, D.; Zhou, X. *Inorg. Chem.* **2012**, *51*, 5208. (b) Lin, C. J.; Chen, C. Y.; Kundu, S. K.; Yang, J. S. *Inorg. Chem.* **2014**, *53*, 737. (c) Liu, Y.; Guo, H.; Zhao, J. *Chem. Commun.* **2011**, *47*, 11471.

(5) (a) Zhang, G.; Palmer, G. M.; Dewhirst, M. W.; Fraser, C. L. *Nat. Mater.* **2009**, *8*, 747. (b) Zhang, S.; Hosaka, M.; Yoshihara, T.; Negishi, K.; Iida, Y.; Tobita, S.; Takeuchi, T. *Cancer Res.* **2010**, *70*, 4490. (c) Zhao, Q.; Zhou, X. B.; Cao, T. Y.; Zhang, K. Y.; Yang, L. J.; Liu, S. J.; Liang, H.; Yang, H. R.; Li, F. Y.; Huang, W. *Chem. Sci.* **2015**, *6*, 1825. (d) Zheng, X.; Wang, X.; Mao, H.; Wu, W.; Liu, B.; Jiang, X. *Nat. Commun.* **2015**, *6*, 5834.

(6) Delor, M.; Keane, T.; Scattergood, P. A.; Sazanovich, I. V.; Greetham, G. M.; Towrie, M.; Meijer, A. J. H. M.; Weinstein, J. A. *Nat. Chem.* **2015**, *7*, 689.

(7) (a) Wilson, J. S.; Chawdhury, N.; Al-Mandhary, M. R.; Younus, M.; Khan, M. S.; Raithby, P. R.; Kohler, A.; Friend, R. H. *J. Am. Chem. Soc.* **2001**, *123*, 9412. (b) Liu, Y.; Jiang, S.; Glusac, K.; Powell, D. H.; Anderson, D. F.; Schanze, K. S. *J. Am. Chem. Soc.* **2002**, *124*, 12412.

(8) Chawdhury, N.; Kohler, A.; Friend, R. H.; Wong, W. Y.; Lewis, J.; Younus, M.; Raithby, P. R.; Corcoran, T. C.; Al-Mandhary, M. R. A.; Khan, M. S. *J. Chem. Phys.* **1999**, *110*, 4963.

(9) Bradshaw, J. D.; Guo, L.; Tessier, C. A.; Youngs, W. J. *Organometallics* **1996**, *15*, 2582.

(10) Alqaisi, S. M.; Galat, K. J.; Chai, M.; Ray, D. G.; Rinaldi, P. L.; Tessier, C. A.; Youngs, W. J. *J. Am. Chem. Soc.* **1998**, *120*, 12149.

(11) (a) Fan, Y.; Zhao, D. *ACS Appl. Mater. Interfaces* **2015**, *7*, 6162. (b) Hua, F.; Kinayyigit, S.; Cable, J. R.; Castellano, F. N. *Inorg. Chem.* **2006**, *45*, 4304. (c) Hua, F.; Kinayyigit, S.; Rachford, A. A.; Shikhova, E. A.; Goeb, S.; Cable, J. R.; Adams, C. J.; Kirschbaum, K.; Pinkerton, A. A.; Castellano, F. N. *Inorg. Chem.* **2007**, *46*, 8771.

(12) Sonogashira, K.; Yatake, T.; Tohda, Y.; Takahashi, S.; Hagihara, N. *J. Chem. Soc., Chem. Commun.* **1977**, 291.

(13) Kuchison, A. M.; Wolf, M. O.; Patrick, B. O. *Inorg. Chem.* **2010**, *49*, 8802.

(14) Johnson, C. A.; Haley, M. M.; Rather, E.; Han, F.; Weakley, T. J. R. *Organometallics* **2005**, *24*, 1161.

(15) (a) Kuchison, A. M.; Wolf, M. O.; Patrick, B. O. *Dalton Trans.* **2011**, *40*, 6912. (b) Cao, Y.; Wolf, M. O.; Patrick, B. O. *Inorg. Chem.* **2013**, *52*, 5636.

(16) Sheng, C. X.; Singh, S.; Gambetta, A.; Drori, T.; Tong, M.; Tretiak, S.; Vardeny, Z. V. *Sci. Rep.* **2013**, *3*, 2653.

(17) Minaev, B.; Jansson, E.; Lindgren, M. *J. Chem. Phys.* **2006**, *125*, 094306.

(18) Boudreault, P.-L. T.; Hennek, J. W.; Loser, S.; Ortiz, R. P.; Eckstein, B. J.; Facchetti, A.; Marks, T. J. *Chem. Mater.* **2012**, *24*, 2929.

(19) Hung, T. Q.; Dang, T. T.; Villinger, A.; Sung, T. V.; Langer, P. *Org. Biomol. Chem.* **2012**, *10*, 9041.

(20) *SAINT*, Version 8.34A; Bruker AXS Inc.: Madison, WI, 1997−2013.

(21) Krause, L.; Herbst-Irmer, R.; Sheldrick, G. M.; Stalke, D. *J. Appl. Crystallogr.* **2015**, *48*, 3.

(22) Sheldrick, G. M. *Acta Crystallogr., Sect. A: Found. Adv.* **2015**, *71*, 3.

(23) Frisch, M. J.; Trucks, G. W.; Schlegel, H. B.; Scuseria, G. E.; Robb, M. A.; Cheeseman, J. R.; Scalmani, G.; Barone, V.; Mennucci, B.; Petersson, G. A.; Nakatsuji, H.; Caricato, M.; Li, X.; Hratchian, H. P.; Izmaylov, A. F.; Bloino, J.; Zheng, G.; Sonnenberg, J. L.; Hada, M.; Ehara, M.; Toyota, K.; Fukuda, R.; Hasegawa, J.; Ishida, M.; Nakajima, T.; Honda, Y.; Kitao, O.; Nakai, H.; Vreven, T.; Montgomery, J. A., Jr.; Peralta, J. E.; Ogliaro, F.; Bearpark, M. J.; Heyd, J.; Brothers, E. N.; Kudin, K. N.; Staroverov, V. N.; Kobayashi, R.; Normand, J.; Raghavachari, K.; Rendell, A. P.; Burant, J. C.; Iyengar, S. S.; Tomasi, J.; Cossi, M.; Rega, N.; Millam, N. J.; Klene, M.; Knox, J. E.; Cross, J. B.; Bakken, V.; Adamo, C.; Jaramillo, J.; Gomperts, R.; Stratmann, R. E.; Yazyev, O.; Austin, A. J.; Cammi, R.; Pomelli, C.; Ochterski, J. W.; Martin, R. L.; Morokuma, K.; Zakrzewski, V. G.; Voth, G. A.; Salvador, P.; Dannenberg, J. J.; Dapprich, S.; Daniels, A.

D.; Farkas, Ö.; Foresman, J. B.; Ortiz, J. V.; Cioslowski, J.; Fox, D. J. *Gaussian 09*, Revision D.01; Gaussian, Inc.: Wallingford, CT, 2009.

(24) (a) Perdew, J. P.; Burke, K.; Ernzerhof, M. *Phys. Rev. Lett.* **1996**, *77*, 3865. (b) Perdew, J. P.; Burke, K.; Ernzerhof, M. *Phys. Rev. Lett.* **1996**, *77*, 3865; *Phys. Rev. Lett.* **1997**, *78*, 1396.

(25) Hay, P. J.; Wadt, W. R. *J. Chem. Phys.* **1985**, *82*, 299.

(26) Miertuš, S.; Scrocco, E.; Tomasi, J. *Chem. Phys.* **1981**, *55*, 117.

(27) Adams, C. J.; Fey, N.; Harrison, Z. A.; Sazanovich, I. V.; Towrie, M.; Weinstein, J. A. *Inorg. Chem.* **2008**, *47*, 8242.

(28) Merrick, J. P.; Moran, D.; Radom, L. *J. Phys. Chem. A* **2007**, *111*, 11683.

DOI: 10.1021/acs.inorgchem.6b01464
Inorg. Chem. XXXX, XXX, XXX−XXX